

Article

Comparing the Field and Laboratory Curing Behaviour of Cold Recycled Asphalt Mixtures for Binder Courses

Gilda Ferrotti ^{1,*} , Andrea Grilli ² , Chiara Mignini ¹  and Andrea Graziani ¹ 

¹ Department of Civil and Building Engineering and Architecture, Polytechnic University of Marche, 60131 Ancona, Italy; c.mignini@pm.univpm.it (C.M.); a.graziani@staff.univpm.it (A.G.)

² Department of Economics, Science and Law, University of the Republic of San Marino, 47890 San Marino City, San Marino; andrea.grilli@unirms.sm

* Correspondence: g.ferrotti@staff.univpm.it

Received: 21 September 2020; Accepted: 19 October 2020; Published: 22 October 2020



Abstract: The cold recycling of reclaimed asphalt (RA) for the rehabilitation of end-of-life pavements is becoming very common. Cold recycled asphalt mixtures (CRAMs) are characterised by a curing time, required to reach the material design mechanical performance. Since the laboratory simulation of the long-term field curing is not yet a standardised procedure, a CRAM was laid as binder course in a full-scale trial section that was monitored for more than two years. The comparison between field curing and oven-curing in laboratory at 40 °C was performed by carrying out indirect tensile stiffness modulus (ITSM), indirect tensile strength (ITS) and complex modulus tests, as well as measurements of the air voids content. The evolution of the ITSM as a function of the curing time (field/oven-curing) was obtained for both gyratory specimens and cores taken from the trial section at different time periods. Results showed that the material stiffness development can be accelerated with a small effect on its long-term value if oven-curing is applied a few days/weeks after compaction. A linear relationship was found between the ITS measured on the cores and their air voids content. Finally, the complex modulus tests confirmed that CRAMs provide an intermediate behaviour between asphalt concrete mixtures and cement-bound mixtures.

Keywords: cold recycling; curing; indirect tensile strength; indirect tensile modulus; reclaimed asphalt; bituminous emulsion

1. Introduction

In the rehabilitation of end-of-life pavements, the focus on cold recycled materials (CRMs) is strongly on the rise, allowing the reuse of reclaimed asphalt (RA) in a cost-effective and environmentally friendly way [1].

The use of different binding agents (i.e., emulsified or foamed bitumen and cement) and their dosages lead to the acquisition of different types of CRM [2], such as bitumen stabilised materials (BSMs), cold recycled asphalt mixtures (CRAMs) and cement-bitumen treated materials (CBTMs) [3,4]. The CRM mechanical behaviour is strictly linked to its composition [5], providing mixtures with properties ranging from those similar to unbound granular materials [6] to those of materials characterised by an intermediate behaviour between cement-bound mixtures [3,7,8] and asphalt concrete (AC). For this reason, several authors have characterised the mechanical behaviour of CRAM by using the complex modulus [9–11]. For CRAMs and CBTMs, the combined effect of bitumen and cement is very effective in terms of water sensitivity [7,8,12–14] and high-temperature stability [12,13,15].

The CRM composition in terms of RA content, is mainly related to the recycling technique [9,16,17]. Cold in-place recycling (CIR) is carried out directly at the jobsite and involves only the bituminous layers. Therefore, the RA aggregate content may reach 100% of the aggregate blend. Full-depth reclamation (FDR) [8,18] is also carried out at the jobsite and involves the full-depth of the pavements, including the bituminous layers and the underlying granular or cemented layers. In this case, the RA content may be reduced to about 30%. Cold central-plant recycling (CCPR) is carried out in a fixed or mobile plant, where selected RA aggregate and virgin aggregate can be combined in the optimal way. The possibility to better control the proportion of the mixture components during material production with CCPR makes this technology able to produce high-performance CRMs for binder and base courses [17].

The selection of the most appropriate CRM composition and recycling technique depends on several factors such as equipment and material availability, thickness and level of the pavement degradation, as well as economic considerations. CRM reaches its design mechanical properties in terms of strength and stiffness only after a specific curing period [19]. Depending on the CRM composition, the curing process results from a combination of several mechanisms such as emulsion breaking, moisture loss and hydration of cementitious compounds [4,7,20–22]. The curing in the field is a gradual process which may require some weeks or even months and is affected by several factors such as temperature, relative humidity, drainage conditions, and layer thickness [4,23]. Specifically, higher temperatures accelerate the curing [23,24], whereas the influence of the relative humidity is mainly linked to the presence of cement [25]. Indeed, a higher humidity promotes the formation of cementitious bonds, thus increasing the material stiffness.

To investigate the long-term performance of the CRMs, the curing is usually accelerated in laboratory by subjecting the specimens to oven-curing at a fixed temperature for several days. Many procedures for curing acceleration exist [26]. The most widespread consists of oven-cure CRM specimens at 40 °C for 3 days immediately after compaction, even if it does not seem to guarantee the achievement of the maximum mixture performance [27].

The main objective of this study was to compare the long-term behaviour of field-cured and laboratory-cured CRAM mixtures. To this end, a trial section was carried out by applying, as binder course, a CRAM produced in an asphalt plant (CCPR technique). Laboratory specimens were compacted immediately after CRAM production and cores were taken from the trial section at several time intervals (up to 796 days after construction). The evolution of the indirect tensile stiffness modulus (ITSM) was studied in different curing conditions: oven-curing at 40 °C, in the field and in a combination of field and oven-curing. Moreover, the relationship between indirect tensile strength (ITS) and air voids content was obtained. Finally, the rheological characterisation of the studied CRAM was performed by measuring and modelling the complex modulus of field specimens.

2. Experimental Program

2.1. Materials and Mixture

The CRAM consists of RA aggregate, virgin river sand, mineral filler, bituminous emulsion, cement and water.

The main characteristics of the RA aggregate and river sand are shown in Tables 1 and 2, respectively. A mineral filler with high fineness (Table 3) was chosen to increase the fine content in the blend and improve the bituminous mastic consistency.

Table 1. Reclaimed asphalt (RA) aggregate characteristics.

Parameter	Standard	Value
Aggregate size (mm)	EN 933-1 [28]	16
Passing at 0.063 mm (%)	EN 933-1 [28]	5.6
Flakiness index (%)	EN 933-3 [29]	7.3
Shape index (%)	EN 933-4 [30]	5.7
Crushed aggregate particle (%)	EN 933-5 [31]	100
Sand Equivalent (%)	EN 933-8 [32]	70.6
Resistance to fragmentation (%)	EN 1097-2 [33]	17
Water absorption (%)	EN 1097-6 [34]	1.3
Bitumen content to mixture (%)	EN 12697-1 [35]	4.1

Table 2. Fine aggregate characteristics.

Parameter	Standard	Value
Fines content (%)	EN 933-1 [28]	2.0
Sand equivalent (%)	EN 933-8 [32]	81
Methylene blue (g/kg)	EN 933-9 [36]	1.2
Density (Saturated surface dry) (Mg/m ³)	EN 1097-6 [34]	2.64
Loose bulk density (Mg/m ³)	EN 1097-3 [37]	1.56
Water absorption (%)	EN 1097-6 [34]	1.0

Table 3. Filler characteristics.

Parameter	Standard	Value
Passing at 2 mm (%)	EN 933-1 [28]	100
Passing at 0.125 mm (%)	EN 933-1 [28]	98
Passing at 0.063 mm (%)	EN 933-1 [28]	95
Methylene blue (g/kg)	EN 933-9 [36]	3.5
Fineness (Blaine) (cm ² /g)	EN 196-6 [38]	6500

An over-stabilised bituminous emulsion, designated as C60B10 (EN 13808 [39]) and a Portland limestone cement, designated as CEM II/B-LL 32.5R (EN 197-1 [40]) were selected as co-binders. Their main characteristics are shown in Tables 4 and 5.

Table 4. Portland cement characteristics.

Parameter	Standard	Value	Specifications
Setting time (min)	EN 196-3 [41]	140	>75
Fineness (Blaine) (cm ² /g)	EN 196-6 [38]	4900	-
Strength after 2 days (MPa)	EN 196-1 [42]	22	>10
Strength after 28 days (MPa)	EN 196-1 [42]	42	≥32.5

Table 5. Bituminous emulsion characteristics.

Parameter	Standard	Value	Specification
pH value (pH)	EN 12850 [43]	2.45	positive
Residual binder (%)	EN 1431 [44]	59.8	60 ± 2
Storage stability (%)	EN 1429 [45]	3	≤10
Breaking value (–)	EN 13075-1 [46]	190	>150
Mixing stability with cement (g)	EN 12848 [47]	<0.2	<2
Characteristic of bitumen (EN 13074 [48])			
Penetration value (mm × 10 ^{−1})	EN 1426 [49]	58	<100
Softening point (°C)	EN 1427 [50]	47.8	>45

The mix design of the CRAMs employed in this research was carried out in accordance with the specifications of the Republic of San Marino road agency [51]. The design aggregate blend was obtained by combining 88% of RA aggregate, 10% of river sand and 2% of filler (Table 6 and Figure 1). The design bituminous emulsion dosage, by dry aggregate mass, was 4.5% and 4.0% (2.7% and 2.4% of residual bitumen) for the mixes employed for the binder and base courses, respectively. The design cement dosage, by dry aggregate mass, was 2.0% and the total water content was 5.0% by dry aggregate mass (including both the emulsion water and prewetting water). At the design composition, the CRAM specimens compacted with a gyratory compactor at 100 gyrations had a dry density of 2.123 Mg/m³ (EN 12697-6 [52]) and an average indirect tensile strength (ITS) (EN 12697-23 [53]) value at 25 °C of 0.41 MPa (curing for 72 h at 40 °C).

Table 6. Design gradation and specification limits.

Sieve Size (mm)	Design Gradation (% Passing)	Specification Limits (% Passing)
31.5	100	100–100
20	99	90–100
16	96	
14	93	
12.5	88	
10	79	50–80
8	71	
6.3	62	
5	54	
4	46	30–55
2	33	20–40
0.5	19	10–25
0.25	16	
0.063	5.1	3–8

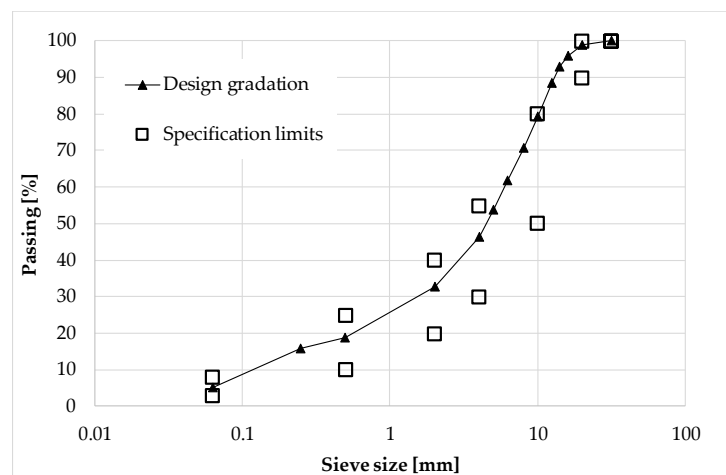


Figure 1. Design gradation.

2.2. Trial Section

2.2.1. Mixing Plant

To produce the CRAM, a mix plant for cement treated mixtures was modified by adding an inlet and storage system for the bituminous emulsion (Figure 2). The emulsion is directly discharged at around 55 °C into the twin-shaft counter-rotating mixer, almost simultaneously with aggregates, filler, cement and water. The mixing requires 20 s and afterwards the cold mixture is transferred into a storage bin before being discharged into waiting trucks. The capacity of the mixing plant is 200 t/h.

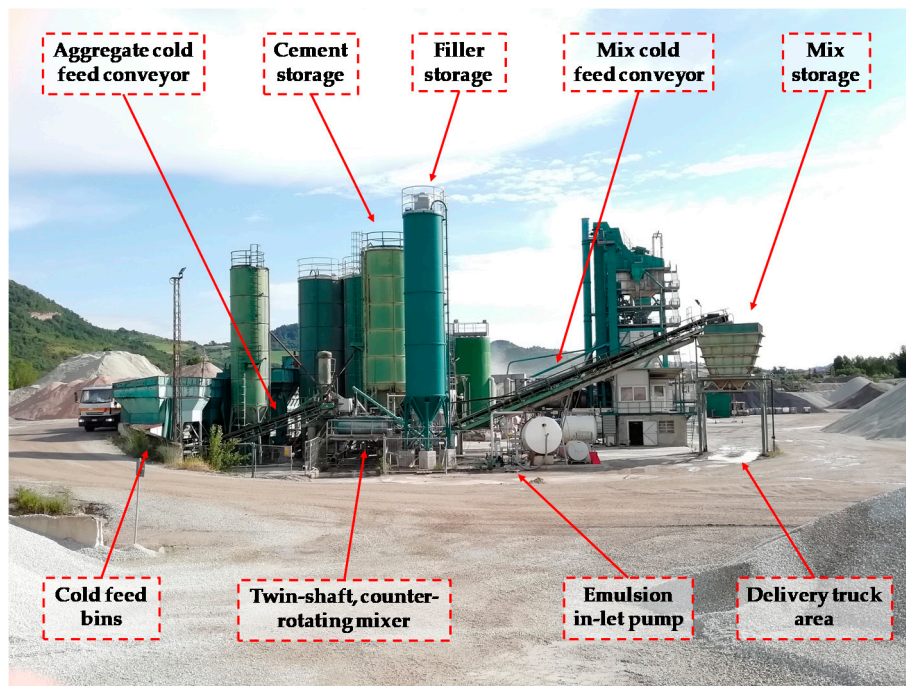


Figure 2. Mixing plant for cold mixture production.

2.2.2. Construction of the Trial Section

The trial section was constructed adjacent to the mixing plant that is located in central-northern Italy, where a Mediterranean climate is present. Since the curing of CRAMs strongly depends on climatic conditions, the daily temperatures and the rainy days were collected at a meteorological station 35 km away from the mixing plant. They are shown in Figure 3, starting from the day of production and laying (24 March 2018) until about 5 months later (31 August 2018).

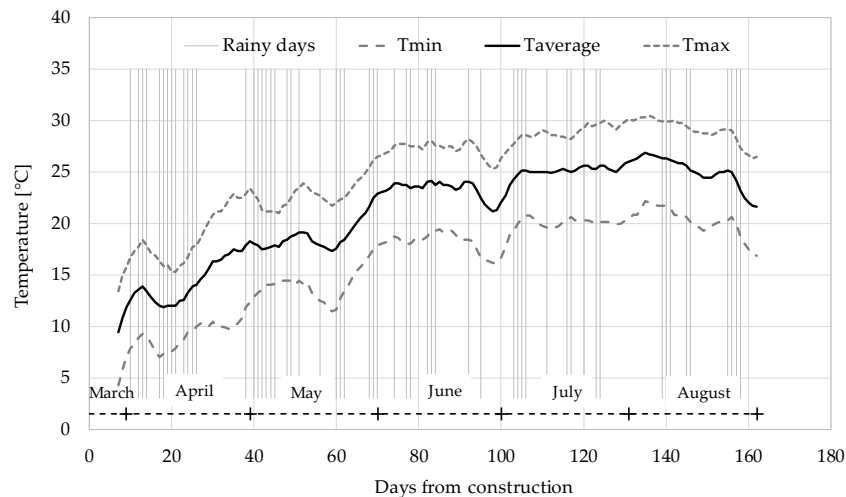


Figure 3. Rainy days (vertical lines) and moving average (period = 7 days) of daily temperatures near the plant.

The trial section (Figure 4), detailedly described by Grilli et al. [54], consists of five subsections (A, B, C, D and E) characterised by different layers (Figure 5) and different compaction procedures of the CRAM binder course (Table 7). Before construction, static plate load tests (DIN 18134 [55]) were performed on the subgrade of all subsections and the E_{v1} modulus results are shown in Figure 5.

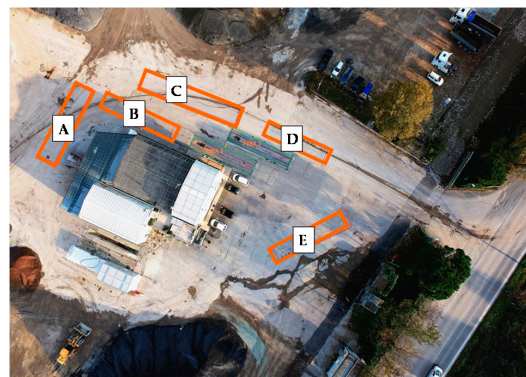


Figure 4. Location of the five Subsections.

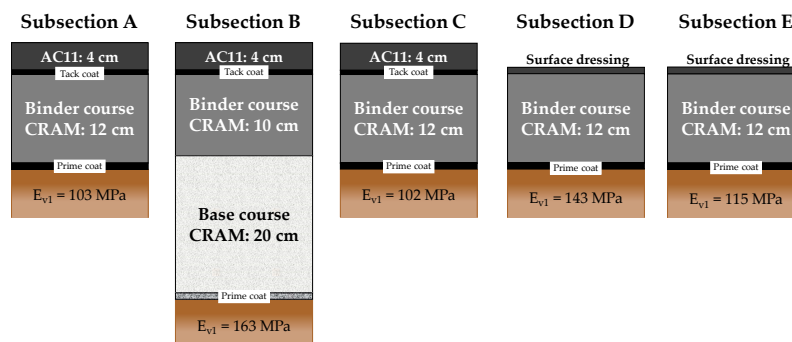


Figure 5. Scheme of the Subsections composition.

Table 7. Compaction procedure of the cold recycled asphalt mixture (CRAM) binder course.

Subsection	First Phase		Second Phase		Third Phase	
	Rolle Type	# Passes	Rolle Type	# Passes	Rolle Type	# Passes
A	9t SR ¹	5	22t PR ²	10	9t SR	5
B	9t SR	5	22t PR	15	9t SR	5
C	22t PR	2	9t SR	5	22t PR	13
D	9t SR	3	22t PR	15		
E	12t SR ³	22				

¹ Nine-ton steel-wheeled roller; ² 22-ton pneumatic-tired roller; ³ 12-ton steel-wheeled roller.

Three types of structure were considered to simulate different maintenance activities provided by the Republic of San Marino road agency:

- Subsections A (17 m long and 5 m wide) and C (25 m long and 4 m wide) represent a typical intermediate maintenance work and consist in 12 cm of CRAM binder course and 4 cm of asphalt concrete wearing course with maximum aggregate size of 11 mm (AC11);
- Subsection B (25 m long and 4 m wide) represents a typical deep maintenance work and consists of 20 cm of CRAM base course, 10 cm of CRAM binder course and 4 cm of AC11 wearing course;
- Subsection D (15 m long and 4 m wide) and E (19 m long and 4 m wide) represent a typical maintenance work for rural roads and consists of 12 cm of CRAM binder course and a double-layered surface dressing.

In all subsections, a bituminous emulsion prime coat (1.00 kg/m² of residual bitumen) was applied above the subgrade and a bituminous emulsion tack coat (0.60 kg/m² of residual bitumen), or a surface treatment, was applied above the CRAM layer, immediately after construction.

Several compaction procedures, in terms of roller weight (9, 12 or 22 tons), roller type (steel or pneumatic) and number of passes (back-forth movement), were considered for the CRAM binder

course to take into account different construction practices (Table 7 and Figure 6). The roller covered the width of the layer in no more than four overlapping passes assuming that the overlap is not less than 20 cm.



Figure 6. Compaction of CRAM binder course of Subsection C by using the 22-ton pneumatic-tired roller.

All the Subsections were opened to traffic 4 days after construction. Traffic data were collected for Subsection B, C and D. After two years from construction, Subsection B was subjected to heavy traffic corresponding to about 270,000 cycles of 80 kN equivalent standard axle load (ESAL) whereas Subsections C and D were subjected to about 70,000 ESAL. No distresses are visible on the Subsections.

2.3. Experimental Program

In this study, only the CRAM applied as binder course (Figure 5) was tested. During the construction of the trial section, the loose mixture was immediately compacted with a gyratory compactor to produce four specimens with a diameter of 150 mm and a height, after 100 gyrations, of about 70 mm. After the trial section construction, 30 cores were taken from the subsections at several time intervals. As shown in Table 8, the cores were divided into groups, based on the coring date. We highlight that Group 2 included cores taken from all subsections, while Subsection C was cored four times, from 23 to 796 days after construction.

Table 8. Coring plan.

Group	Coring Date (mm/dd/yy)	Days from Construction	Core Diameter (mm)	Number of Specimens				
				Subsections				
				A	B	C	D	E
1.1	16 April 2018	23	150	-	-	3	-	-
1.2	16 April 2018	23	200	-	1	2	-	-
2	5 June 2018	73	134	3	3	3	3	3
3	28 August 2018	157	134	-	3	3	-	-
4	28 May 2018	796	134	-	-	3	-	-

The gyratory specimens (Group 0) and the core specimens of Groups 1.1 and 2 were oven-cured in the laboratory at 40 °C and tested at different curing periods (Figure 7) for monitoring the evolution of the ITSM. At the end of the selected curing period, the ITS was measured on all specimens. After testing, the volumetric characterisation of Group 0 and Group 2 specimens was performed 157 days after construction, when most of (or all) the hydration had occurred, according to EN 12697-6 [52] (Procedure C, i.e., sealed specimen method) and EN 12697-8 [56].

The three cores of Group 1.2 were cured at room temperature and subjected to complex modulus testing. The cores of Groups 3 and 4 were tested (ITSM and ITS) immediately after coring (Figure 7).

We highlight that the humidity of the CRAM subjected to oven-curing and free evaporation (in laboratory) was totally different from the field, where evaporation is restricted as the mixture was sealed between two bituminous layers (prime coat and tack coat/surface dressing).

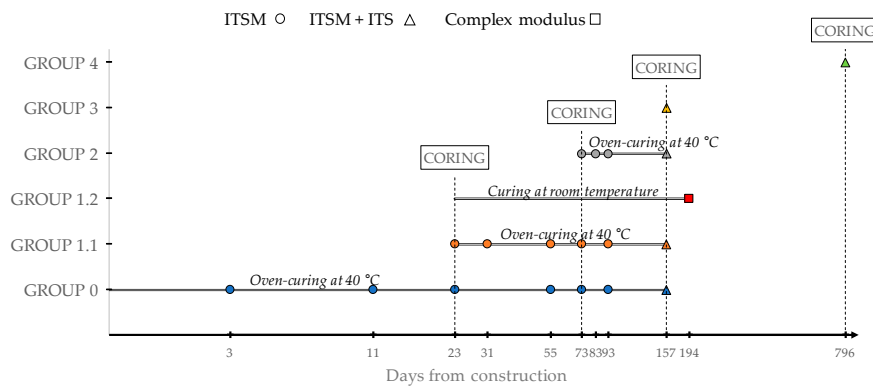


Figure 7. Experimental program.

2.4. Testing Procedures

The ITSM test was carried out at 20 °C, according to EN 12697-26 (Annex C) [57]. The ITSM was measured as average value after the application of five load pulses with a rise time of 124 ms. Two orthogonal diameters were tested for each cylindrical specimen and the average ITSM was calculated.

The ITS test was carried out at 20 °C, according to EN 12697-23 [53]. The test allows the calculation of the tensile strength of a cylindrical specimen, loaded diametrically until its failure.

The complex modulus was measured on cylindrical specimens with a diameter of 75 mm and a height of 140 mm, obtained with an additional horizontal coring from cores of Group 1.2 (Figure 8a). The test was carried out with the asphalt mixtures performance tester (AMPT Pro). During the test, a strain amplitude of 30 microstrain was kept constant by applying a haversine compression load. Three linear variable differential transformers (LVDT) placed 120° apart (Figure 8b) were used for measuring the axial strain on the middle part of the specimen, while a load cell was employed for axial stress measurement. Five temperatures (0, 10, 20, 35, 50 °C), five frequencies (0.1, 0.5, 1, 5, 10 Hz) and 20 loading cycles for each frequency were applied, allowing the determination of the stiffness modulus E_0 and phase angle φ .



Figure 8. (a) Horizontal coring from core of 200-mm diameter; (b) detail of the specimen mounted in the asphalt mixtures performance tester (AMPT Pro).

3. Results and Discussion

3.1. Volumetric Characterisation

The bitumen content, recovered from the loose CRAM binder material after in-plant production, was equal to 5.9% with respect to the mixture mass. The air voids content of the CRAM specimens included in Group 0 and Group 2 is shown in Table 9 (average value of 2 or 3 replicates). The air

voids of Subsections A, B and C are similar (around 15.5%) and do not allow different site compaction practices to be distinguished. Subsection D, where the least number of passes was carried out (Table 7), provided the highest air voids content (17.0%). On the contrary, Subsection E, where only the 22-ton steel roller was used, provided the lowest air voids content (14.1%).

Table 9. Air voids content of CRAM binder specimens of Group 0 and Group 2.

Specimens	Air Voids Content	
	Average Value (%)	Max-Min (%)
Gyratory	11.8	0.853
Subsection A	15.9	0.789
Subsection B	15.4	1.278
Subsection C	15.5	0.642
Subsection D	17.0	0.561
Subsection E	14.1	1.008

Apparently, there is a correlation between the air voids of the cores and the number of roller passes. However, we underline that other factors may have influenced the volumetric properties of the specimens, such as the subgrade bearing capacity (existing base course or new CRAM base course) and the post-compaction due to heavy vehicle circulation on the various subsections.

Gyratory specimens provided significantly lower air voids content (11.8%) than core specimens. This suggests that the adopted compaction energy (100 gyrations), which was required by the construction specification [51], overestimates the actual field compaction effort provided by the rollers.

3.2. Mechanical Characterisation

3.2.1. ITSM Test Results

Figure 9 shows the relationship between ITSM at 20 °C and air voids content of cores of Group 2, at different curing conditions. Each point is the average value of three specimens (Table 8).

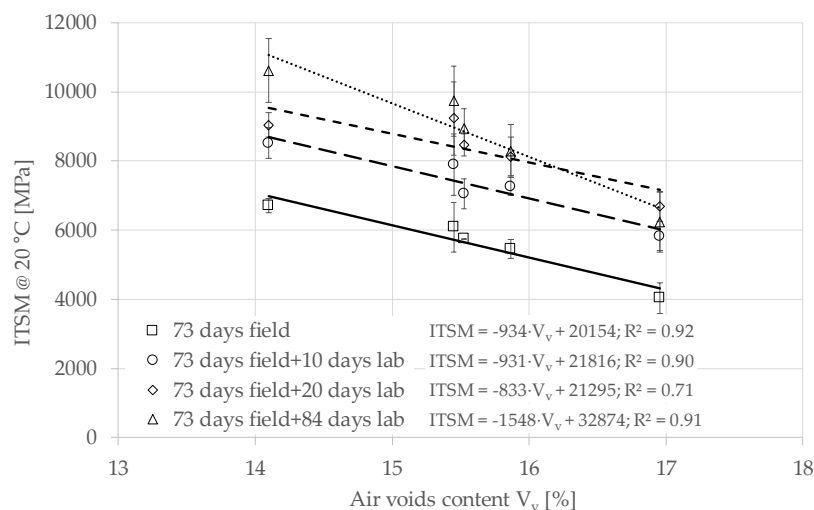


Figure 9. Relationship between indirect tensile stiffness modulus (ITSM) and air voids content of specimens of Group 2 at different curing times.

The ITSM can be considered linearly dependent on the air voids in all the curing conditions. Results from tests until 93 days after construction (73 days field + 20 days lab), indicate that the curing did not affect the linear correlation between ITSM and air voids. Specifically, a 1% increase in air voids led to a reduction of ITSM of about 900 MPa. Results from tests after a 157-day curing time (73 days

field + 84 days lab) kept an almost linear trend but with a higher sensibility to the air voids. This is probably due to the replication of the ITSM tests on the same cores, which may have reduced the stiffness of the cores characterised by a higher air voids (Subsection D with 17% of air voids content).

Figure 10 shows the evolution of the average ITSM values over the curing time for gyratory specimens (Group 0) and core specimens of Group 2. The experimental data were fitted through the asymptotic model proposed by Graziani et al. [23,58]:

$$y(t) = y_i + (y_a - y_i) \frac{t - t_i}{(h_y - t_i) + (t - t_i)} \tag{1}$$

where t (days) is the curing time, $y(t)$ is the property under investigation (ITSM), t_i is the curing time when the property was measured for the first time (i.e., 3 or 73 days), y_i is an intercept term that represents the value of the properties at the time t_i , y_a is the long-term asymptotic value of $y(t)$ and h_y (days) is a parameter representing a specific curing time. The parameter y_i gives information on the average rate of evolution of the material properties from the day of construction to t_i .

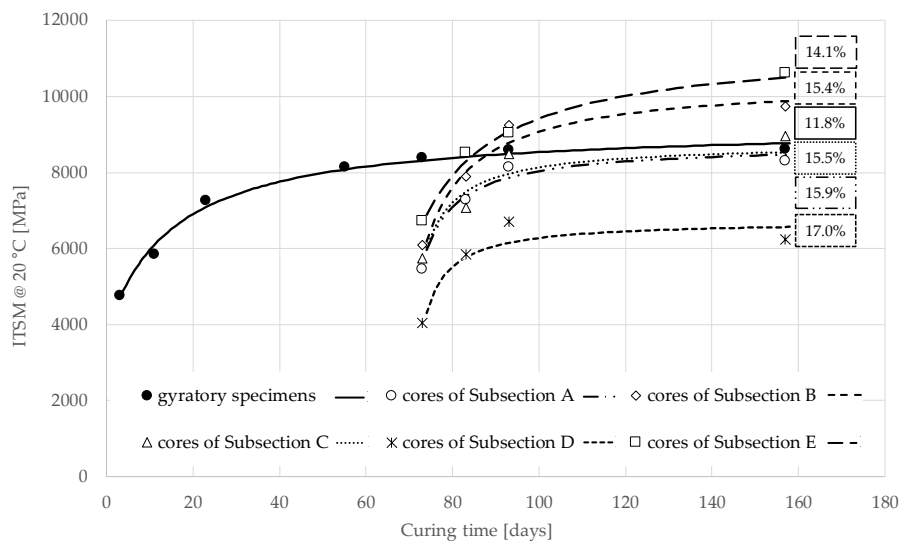


Figure 10. Measured data and model of the evolution of ITSM over curing time for specimens of Group 0 (gyratory) and Group 2 (cores).

The agreement between the measured data and the estimated regression curves is quite good, as shown in Figure 10 and Table 10, where the estimated values of the regression parameters are reported along with the coefficient of determination R^2 and the air voids.

Table 10. Estimated values of the regression parameters and air voids content of specimens of Group 0, Group 1.1, Group 2 and field curing.

Specimen Type	t_i (Days)	y_i (MPa)	y_a (MPa)	h_y (Days)	R^2 (-)	Air Voids Content (%)
gyratory specimens	3	4668	9246	21	0.97	11.8
cores of Sub. A-Group 2	73	5603	8730	81	0.85	15.9
cores of Sub. B-Group 2	73	5807	10,412	84	0.75	15.4
cores of Sub. C-Group 2	73	5625	8775	80	0.85	15.5
cores of Sub. D-Group 2	73	3815	6729	78	0.70	17.0
cores of Sub. E-Group 2	73	6643	11,375	92	0.89	14.1
cores of Sub. C-Group 1.1	23	4139	8415	35	0.94	-
cores of Sub. C-field curing	23	3850	8001	69	0.94	-

The gyratory specimens of Group 0 and the cores of Group 2 showed a different evolution of ITSM. The gyratory specimens, oven-cured in laboratory at 40 °C starting immediately after production, showed a rapid increase in stiffness in the first days, with the ITSM reaching about 4500 MPa after 3 days and 7200 MPa after 21 days. At longer curing times, the stiffness increase slowed down, with the ITSM reaching about 8200 MPa after 73 days and a long-term asymptotic value of 9246 MPa (Table 10).

For the cores, we have the first ITSM measurement after 73 days of field curing, with values ranging from about 4000 (Subsection D) to 6500 MPa (Subsection E). At this curing time, the difference in ITSM between cores and gyratory specimens, is due to differences in both volumetric properties (the cores had higher voids) and curing conditions (oven-curing vs. field curing). The effect of air voids can be estimated using the experimental data reported in Figure 9. Specifically, with an air voids content of 11.8% we can extrapolate an ITSM of about 9100 MPa after 73 days of field curing. Such value is even higher than the ITSM measured on the gyratory specimens. We can conclude that, in these in-situ conditions (pavement stratigraphy, location and climate), field curing did not penalise the stiffness evolution until 73 days. This tendency is confirmed in the long-term. In fact, Figure 10 shows that the core specimens, which were oven-cured at 40 °C after extraction, had a rapid increase in stiffness and reached an asymptotic value of ITSM ranging from 6729 (Subsection D) to 11,375 MPa (Subsection E). We observe that the asymptotic value of the gyratory specimens is comprised in this range, although they had lower air voids.

The field curing curve shown in Figure 11 depicts the ITSM evolution observed on core specimens taken from Subsection C, from 23 to 796 days after construction, when also field ageing, moisture damage and traffic induced stress influenced the material performance. These measurements reveal the actual stiffness evolution of the material in the field. This trend is compared with the stiffness evolution observed on cores taken 23 days (Group 1.1) and 73 days (Group 2 Sub. C) after construction and then oven-cured at 40 °C. The measurements were fitted using the model described in Equation (1) and the estimated values of the regression parameters are reported in Table 10. The core specimens taken after 23 and 73 days and oven-cured at 40 °C show a rapid increase in stiffness and, in the long term, they are characterised by similar asymptotic values of ITSM: 8415 MPa and 8775 MPa, respectively. These values are only slightly higher than the asymptotic value which characterises the field cured material, 8001 MPa.

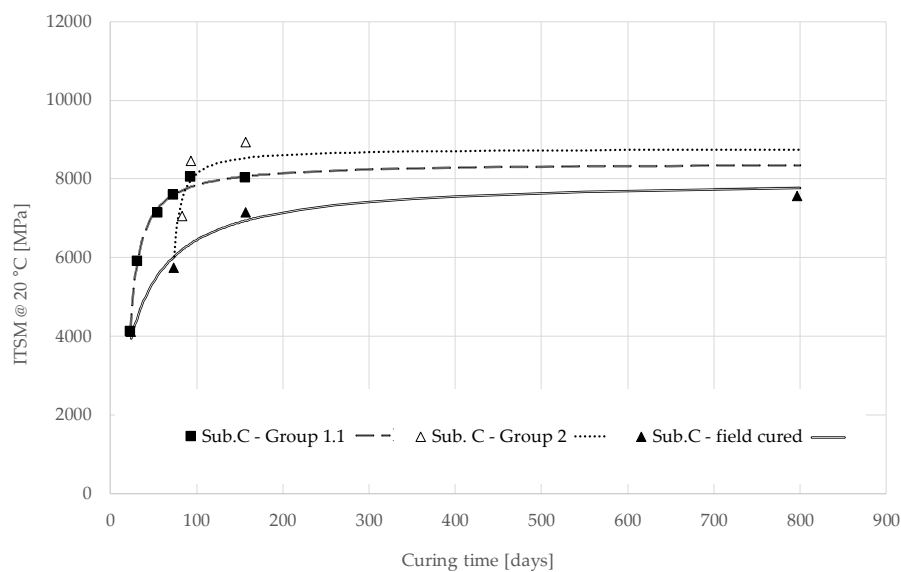


Figure 11. Measured data and model of the evolution of ITSM over curing time for core specimens of Subsection C: Group 1.1, Group 2 and field curing.

In summary, oven-curing with free evaporation and high temperature (40 °C), a procedure that is often used for accelerated curing in the laboratory, may lead to an underestimation of the long-term stiffness of the mixture cured in the field with restricted evaporation (Figure 10). On the other hand, if oven-curing is applied after a few days or weeks of field curing with restricted evaporation, the long-term stiffness will not be affected (Figure 11). This is because the humidity of the material subjected to oven-curing and free evaporation may be totally different from the field. Therefore, the evolution of the cementitious and bituminous bonds will be different because humidity enhances the former and penalises the latter.

These results suggest that the curing conditions immediately after compaction determine the microstructure of the material (distribution and location of cementitious and bituminous bonds). With immediate oven-curing and free evaporation (laboratory conditions), bituminous bonds are favoured with respect to cementitious bonds, whereas if evaporation is restricted (field curing), the cementitious bonds are favoured leading to a higher long-term stiffness. When oven-curing is applied a few days/weeks after compaction (i.e., when the mixture microstructure is already formed in sealed conditions), the stiffness development will be accelerated with a small effect on its long-term value.

3.2.2. ITS Results

Figure 12 shows the results of the ITS tests performed on the core specimens of Group 2, cured 73 days in the field and then 84 days in laboratory at 40 °C, and on the gyratory specimens cured 157 days in laboratory at 40 °C. A linear relationship is found between the ITS of the cores and their air voids content. Specifically, a 3% increase in air voids led to approximately a halving of ITS (from 0.69 to 0.38 MPa). This trend shows that if hypothetical cores with an air void content of 11.8% (corresponding to the value obtained for the gyratory specimens) were considered, the ITS value would be considerably higher than that provided by the gyratory specimens. This confirms what was already observed during ITSM tests: the combination of field and laboratory curing would lead to a different structure compared to the sole curing in the laboratory at 40 °C.

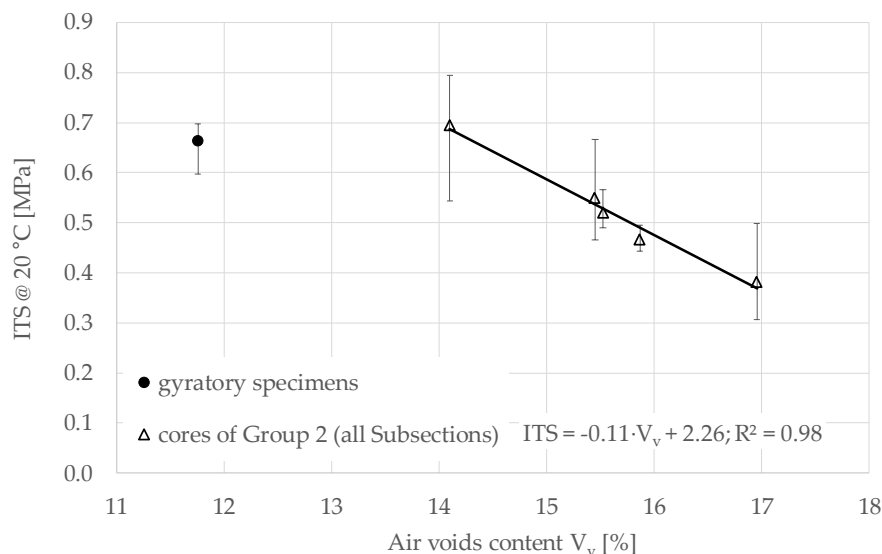


Figure 12. Indirect tensile strength (ITS) (with max and min error bars) as a function of air voids, 157 days after construction.

3.2.3. Complex Modulus

Figure 13 shows the complex modulus results obtained on cores extracted from Subsections B (B10, with air voids content of 14.3%) and C (C12 and C13, with air voids contents of 18.4% and 18.9%,

respectively). The results are plotted in the Black diagram (stiffness modulus E_0 as a function of the phase angle ϕ —Figure 13a) and in the Cole–Cole diagram (loss modulus E_2 as a function of storage modulus E_1 —Figure 13b).

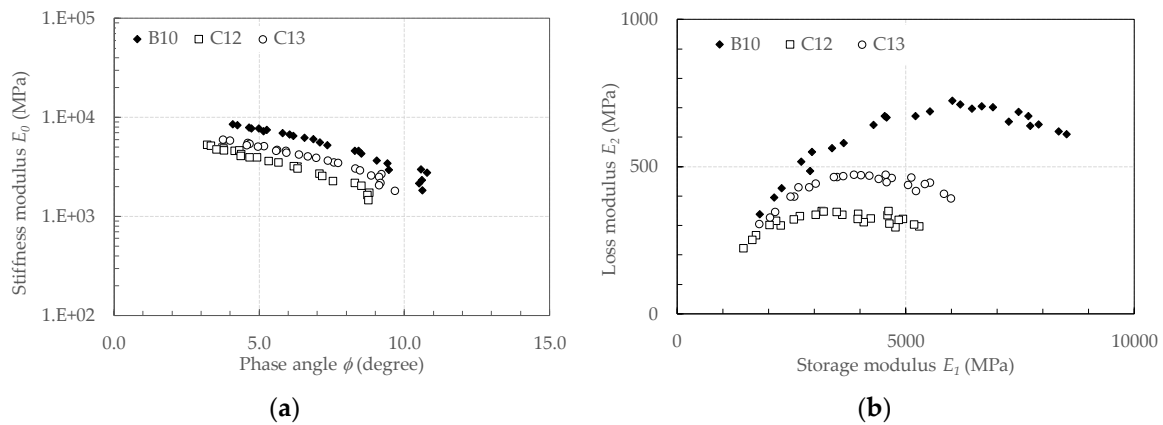


Figure 13. Measured values of E_0 for CRAM: (a) Black diagram; (b) Cole–Cole diagram

Overall, the stiffness modulus was comprised between 9500 (B10, $T = 0^\circ\text{C}$, $f = 10\text{ Hz}$), and 1500 MPa (C12, $T = 50^\circ\text{C}$, $f = 0.1\text{ Hz}$). This range of variation is less than one order of magnitude, whereas, in the same temperature and frequency range, conventional AC mixtures normally show a variability of more than two orders of magnitude [59]. Concurrently, the values of the phase angle were less than about 10° . These reduced ranges of variability characterise the typical behaviour of cold recycled mixtures where cement plays an important role in limiting the thermo-viscoelastic behaviour [60].

For each specimen, a loading frequency increase (or decrease) had the same effect on E^* as the temperature decrease (or increase). This confirms the validity of the time-temperature superposition principle (TTSP). In other terms, despite the concurrent presence of the residual bitumen from the emulsion and the aged bitumen of the RA aggregates, the tested CRAMs showed a thermo-rheologically simple behaviour. The master curves of the stiffness modulus and phase angle were obtained by fixing the reference temperature $T_0 = 20^\circ\text{C}$ and shifting the experimental data along the frequency axis until obtaining continuous curves. For each testing temperature T the amount of shifting, i.e., the shift factors $a_0(T)$, was obtained through the closed form shifting (CFS) algorithm, consisting in the minimisation of the area between two adjacent isothermal curves of E_0 [61]. The same shift factors were used also for shifting the ϕ values.

Rheological modelling was carried out using the model proposed by Graziani et al. [10,11] that combines viscoelastic and hysteretic dissipation mechanisms. The viscoelastic part is represented by the Huet–Sayegh (HS) model [62] while the hysteretic part (HY) is represented by a time- and temperature-independent phase angle (ϕ_{HY}). The model, abbreviated HS-HY, is described by the following equation:

$$E_{HS-HY}^*(\omega) = \left[E_e + \frac{E_g - E_e}{1 + \delta(j\omega\tau)^{-k} + (j\omega\tau)^{-h}} \right] \cdot \exp(j\phi_{HY}) \quad (2)$$

where the term in square brackets describes the HS model, and the term $\exp(j\phi_{HY})$ represents a rotation in the complex plane (Figure 14). Physically, the phase angle ϕ_{HY} accounts for the time-independent (non-viscous) and temperature-independent dissipation phenomena which are present during cyclic loading. The term hysteretic is normally used to indicate this type of dissipation mechanism that may be attributed to the cementitious bonds or to internal friction phenomena [63,64].

In Equation (2), j is the imaginary unit and ω is the angular frequency ($\omega = 2\pi f$). E_e is the equilibrium value of E^* ($\omega\tau \rightarrow 0$) and represents the purely elastic material response when the bitumen is liquid, and its contribution to stiffness vanishes (high temperature/low frequency). For AC

mixtures this value represents the interlock between aggregates [65] and for CRAMs it also accounts for the effect of cementitious bonds. E_g is the glassy value of E^* ($\omega\tau \rightarrow \infty$) and represents the purely elastic material response when the bitumen is a glassy solid (low temperature/high frequency). Its value is mainly affected by the volumetric properties of the mixture [66].

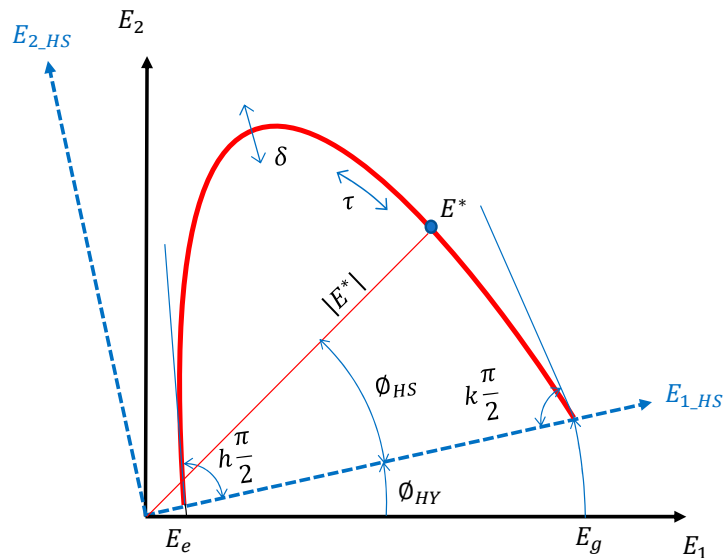


Figure 14. Comparison between the Huet–Sayegh (HS) and HS-HY model.

The dimensionless parameters k , δ and h control the shape of the model in the low, intermediate and high temperature range [67]. Higher values of h and k indicate that a higher viscous dissipation component is present in the material response (with one indicating purely viscous behaviour). On the other hand, lower values of h and k indicate that the material response is more elastic (with zero indicating purely elastic behaviour). In general, physically consistent values are $0 < k < h < 1$, with k characterising the low temperature/high frequency behaviour and h the high temperature/low frequency behaviour.

The characteristic time τ is a function of the testing temperature:

$$\tau = \tau_0 \cdot a_0(T) \tag{3}$$

where τ_0 is the characteristic time at the reference temperature. The value of τ does not affect the shape of the master curves. In fact, since τ is a frequency multiplier, it only affects the position of the master curve along the frequency axes. If τ increases, the E_0 master curve shifts to the left indicating a lower relaxation ability of the material. Higher values of τ have been correlated to higher degree of bitumen aging and higher RA content, in both hot and cold mixtures [10,68–70].

Figure 15a shows the master curves superimposed to the experimental data and the shift factors, whereas Table 11 summarises the model parameters. The E_e values of the three specimens are very similar, confirming that they were obtained from the same mixture (same aggregate composition, same amount of cement). Very similar E_g values were obtained for C12 e C13 specimens whereas B10 specimen provided a higher value, probably due to a lower air voids content of B10 (14.3%) with respect to C12 and C13 (18.4 and 18.9%, respectively).

Identical values of h and k were used for all specimens, obtaining an excellent fitting of the experimental data. This indicates that when $\omega\tau \rightarrow 0$ (high temperature/low frequency) and $\omega\tau \rightarrow \infty$ (low temperature/high frequency) the specimens showed the same viscoelastic dissipation behaviour. The variability of τ_0 may be explained by specimen-to-specimen variability.

The values of ϕ_{HY} are comprised between 0.7° and 1.5° , whereas the measured phase angle ranges from 3° to 11° (Figure 15b). Its means that the ratio ϕ_{HY}/ϕ varies from less than 10% (high temperature/low

frequency) to about 30% (high temperature/low frequency). We may conclude that the hysteretic dissipation component represents an important part of the material dissipation behaviour and, more in general, the material is characterised by an intermediate behaviour between AC mixtures and cement-bound mixtures.

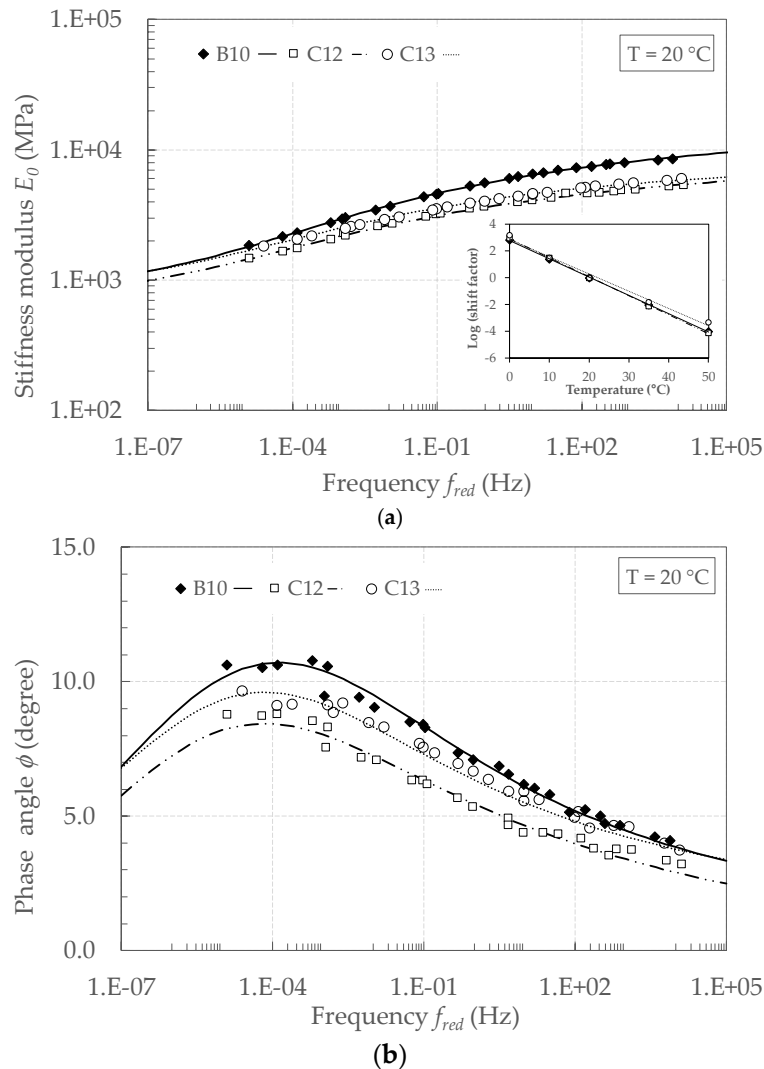


Figure 15. Master curves of CRAM at 20 °C: (a) stiffness modulus E_0 ; (b) phase angle ϕ .

Table 11. Huet–Sayegh model parameters ($T_{ref} = 20\text{ °C}$).

Specimen	E_g (MPa)	E_e (MPa)	k -	h -	δ -	$\log \tau_0$ -	ϕ_{HY} (°)
B10	13,583	833	0.093	0.265	1.819	0.669	0.701
C12	7921	712	0.093	0.265	1.990	1.420	0.147
C13	7943	861	0.093	0.265	1.600	1.566	1.439

4. Conclusions

This study aimed at comparing the oven-curing in laboratory and the field curing of a CRAM mixture, laid in a full-scale trial section. The CRAM was produced with the CCPR technique and applied as binder course. Gyratory compacted specimens and cores taken from the pavement at different time intervals were investigated for more than two years.

The results show that the air voids content strongly affects the mechanical properties of CRAMs. Linear relationships link both ITSM and ITS to the air voids content, by showing that the production of

laboratory specimen with a correct air voids level is essential for estimating the mixture performance in the field.

The evolution of the average ITSM values over the curing time was fitted with an asymptotic model, which was in good agreement with the measured data. The differences in curing procedures between laboratory and field caused differences in ITSM. This suggests that oven-curing with free evaporation (laboratory) and sealed curing with restricted evaporation (field) led to the formation of a different microstructure. Thus, when bitumen emulsion and cement are used as co-binders, laboratory curing should be carried out both in sealed and unsealed condition to have a complete understanding of the mixture potential behaviour in the field.

The complex modulus results confirmed the validity of the time-temperature superposition principle. A rheological model, explicitly considering non-viscous dissipation, was adopted for analysing the data and confirmed that CRAMs are characterised by an intermediate behaviour between AC and cement-bound mixtures.

This study showed that an additional effort is necessary to find a more effective procedure for producing CRAM specimens in laboratory, able to appropriately estimate the field material performance.

Author Contributions: Conceptualization, A.G. (Andrea Grilli); Methodology, A.G. (Andrea Graziani) and C.M.; Formal Analysis, G.F. and A.G. (Andrea Graziani); Investigation, C.M.; Writing—Original Draft Preparation, G.F.; Writing—Review & Editing, G.F., A.G. (Andrea Grilli), C.M. and A.G. (Andrea Graziani); Supervision, A.G. (Andrea Graziani). All authors have read and agreed to the published version of the manuscript.

Funding: This research received no external funding.

Acknowledgments: The authors wish to thank the Impianti Cave Romagna s.r.l. for the support and collaboration in managing and building the trial section and Valli Zabban S.p.A. for the support in the specific design and qualification of the bituminous emulsion.

Conflicts of Interest: The authors declare no conflict of interest.

Acronyms

The following acronyms were used in the text

Definition	Acronym
closed form shifting algorithm	CFS
cold central-plant recycling	CCPR
cold recycled asphalt mixture	CRAM
cold recycled material	CRM
cold in-place recycling	CIR
full-depth reclamation	FDR
Huet–Sayegh model	HS
indirect tensile stiffness modulus	ITSM
indirect tensile strength	ITS
linear variable differential transformers	LVDT

References

1. Asphalt Recycling and Reclaiming Association (ARRA). *Manual, Basic Asphalt Recycling*; ARRA: Annapolis, MD, USA, 2001.
2. Grilli, A.; Bocci, E.; Graziani, A. Influence of reclaimed asphalt content on the mechanical behaviour of cement-treated mixtures. *Road Mater. Pavement Des.* **2013**, *14*, 666–678. [[CrossRef](#)]
3. Grilli, A.; Graziani, A.; Bocci, M. Compactability and thermal sensitivity of cement-bitumen treated materials. *Road Mater. Pavement Des.* **2012**, *13*, 599–617. [[CrossRef](#)]
4. Cardone, F.; Grilli, A.; Bocci, M.; Graziani, A. Curing and temperature sensitivity of cement-bitumen treated materials. *Int. J. Pavement Eng.* **2015**, *16*, 868–880. [[CrossRef](#)]
5. Kuchiishi, A.K.; Santos Antão, C.C.D.; Vasconcelos, K.; Bernucci, L.L.B. Influence of viscoelastic properties of cold recycled asphalt mixtures on pavement response by means of temperature instrumentation. *Road Mater. Pavement Des.* **2019**, *20* (Suppl. 2), S710–S724. [[CrossRef](#)]

6. Guatimosim, F.V.; Vasconcelos, K.L.; Bernucci, L.L.B.; Jenkins, K.J. Laboratory and field evaluation of cold recycling mixture with foamed asphalt. *Road Mater. Pavement Des.* **2018**, *19*, 385–399. [CrossRef]
7. Bocci, M.; Grilli, A.; Cardone, F.; Graziani, A. A study on the mechanical behaviour of cement-bitumen treated materials. *Constr. Build. Mater.* **2011**, *25*, 773–778. [CrossRef]
8. Godenzoni, C.; Graziani, A.; Bocci, E.; Bocci, M. The evolution of the mechanical behaviour of cold recycled mixtures stabilised with cement and bitumen: Field and laboratory study. *Road Mater. Pavement Des.* **2018**, *19*, 856–877. [CrossRef]
9. Schwartz, C.W.; Diefenderfer, B.K.; Bowers, B.F. *Material Properties of Cold in-Place Recycled and Full-Depth Reclamation Asphalt Concrete*; Transportation Research Board: Washington, DC, USA, 2017.
10. Graziani, A.; Mignini, C.; Bocci, E.; Bocci, M. Complex modulus testing and rheological modeling of cold-recycled mixtures. *J. Test. Eval.* **2020**, *48*, 120–133. [CrossRef]
11. Graziani, A.; Raschia, S.; Mignini, C.; Carter, A.; Perraton, D. Use of fine aggregate matrix to analyze the rheological behavior of cold recycled materials. *Mater. Struct.* **2020**, *53*, 1–16. [CrossRef]
12. Pi, Y.; Huang, Z.; Pi, Y.; Li, G.; Li, Y. Composition Design and Performance Evaluation of Emulsified Asphalt Cold Recycled Mixtures. *Materials* **2019**, *12*, 2682. [CrossRef]
13. Yang, Y.; Yang, Y.; Qian, B. Performance and Microstructure of Cold Recycled Mixes Using Asphalt Emulsion with Different Contents of Cement. *Materials* **2019**, *12*, 2548. [CrossRef] [PubMed]
14. Sangiorgi, C.; Tataranni, P.; Simone, A.; Vignali, V.; Lantieri, C.; Dondi, G. A laboratory and field evaluation of Cold Recycled Mixture for base layer entirely made with Reclaimed Asphalt Pavement. *Constr. Build. Mater.* **2017**, *138*, 232–239. [CrossRef]
15. Li, Y.; Lyv, Y.; Fan, L.; Zhang, Y. Effects of Cement and Emulsified Asphalt on Properties of Mastics and 100% Cold Recycled Asphalt Mixtures. *Materials* **2019**, *12*, 754. [CrossRef] [PubMed]
16. Apeageyi, A.K.; Diefenderfer, B.K. Evaluation of Cold In-Place and Cold Central-Plant Recycling Methods Using Laboratory Testing of Field-Cored Specimens. *J. Mater. Civ. Eng.* **2013**, *25*, 1712–1720. [CrossRef]
17. Timm, D.H.; Diefenderfer, B.K.; Bowers, B.F. Cold central plant recycled asphalt pavements in high traffic applications. *Transp. Res. Record* **2018**, *2672*, 291–303. [CrossRef]
18. Bocci, M.; Grilli, A.; Cardone, F.; Ferrotti, G. Full-depth reclamation for the rehabilitation of local roads: A case study. *Int. J. Pavement Eng.* **2014**, *15*, 191–201. [CrossRef]
19. Jenkins, K.J. Mix Design Considerations for Cold and Half-Warm Bituminous Mixes with Emphasis on Foamed Bitumen. Ph.D. Thesis, University of Stellenbosch, Stellenbosch, South Africa, 2000. Available online: <http://scholar.sun.ac.za/handle/10019.1/51831> (accessed on 21 October 2020).
20. Asphalt Academy. *Technical Guideline (TG2): Bitumen Stabilized Materials*, 2nd ed.; Asphalt Academy: Pretoria, South Africa, 2009.
21. Jenkins, K.J.; Moloto, P.K. Updating bituminous stabilized materials guidelines: Mix design report. Phase II—Curing protocol: Improvement. In *Technical Memorandum Task 7*; Jones Edmunds: Gainesville, FL, USA, 2008.
22. Kavussi, A.; Modarres, A. A model for resilient modulus determination of recycled mixes with bitumen emulsion and cement from ITS testing results. *Constr. Build. Mater.* **2010**, *24*, 2252–2259. [CrossRef]
23. Graziani, A.; Godenzoni, C.; Cardone, F.; Bocci, M. Effect of curing on the physical and mechanical properties of cold-recycled bituminous mixtures. *Mater. Des.* **2016**, *95*, 358–369. [CrossRef]
24. Du, S. Effect of curing conditions on properties of cement asphalt emulsion mixture. *Constr. Build. Mater.* **2018**, *164*, 84–93. [CrossRef]
25. Garcia, A.; Lura, P.; Partl, M.N.; Jerjen, I. Influence of cement content and environmental humidity on asphalt emulsion and cement composites performance. *Mater. Struct.* **2013**, *46*, 1275–1289. [CrossRef]
26. Kuchiishi, A.K.; Santos Antão, C.C.D.; Vasconcelos, K.; Pires, J.; de Araújo, O.M.O.; Bernucci, L.L.B.; Lopes, R.T. Investigation of the matric suction role on the curing mechanism of foamed asphalt stabilised mixtures. *Road Mater. Pavement Des.* **2019**, *20* (Suppl. 1), S365–S389. [CrossRef]
27. Meocci, M.; Grilli, A.; La Torre, F.; Bocci, M. Evaluation of mechanical performance of cement-bitumen-treated materials through laboratory and in-situ testing. *Road Mater. Pavement Des.* **2018**, *18*, 376–389. [CrossRef]
28. European Committee for Standardization. *EN 933-1: Tests for Geometrical Properties of Aggregates. Part 1: Determination of Particle Size Distribution—Sieving Method*; European Committee for Standardization: Brussels, Belgium, 2012.
29. European Committee for Standardization. *EN 933-3: Tests for Geometrical Properties of Aggregates. Part 3: Determination of Particle Shape—Flakiness Index*; European Committee for Standardization: Brussels, Belgium, 2012.

30. European Committee for Standardization. *EN 933-4: Tests for Geometrical Properties of Aggregates. Part 4: Determination of Particle Shape—Shape Index*; European Committee for Standardization: Brussels, Belgium, 2008.
31. European Committee for Standardization. *EN 933-5: Tests for Geometrical Properties of Aggregates. Part 5: Determination of Percentage of Crushed and Broken Surfaces in Coarse Aggregate Particles*; European Committee for Standardization: Brussels, Belgium, 2008.
32. European Committee for Standardization. *EN 933-8: Tests for Geometrical Properties of Aggregates. Part 8: Assessment of Fines—Sand Equivalent Test*; European Committee for Standardization: Brussels, Belgium, 2015.
33. European Committee for Standardization. *EN 1097-2: Tests for Mechanical and Physical Properties of Aggregates. Part 2: Methods for the Determination of Resistance to Fragmentation*; European Committee for Standardization: Brussels, Belgium, 2020.
34. European Committee for Standardization. *EN 1097-6: Tests for Mechanical and Physical Properties of Aggregates. Part 6: Determination of Particle Density and Water Absorption*; European Committee for Standardization: Brussels, Belgium, 2020.
35. European Committee for Standardization. *EN 12697-1: Bituminous Mixtures—Test Methods for Hot Mix Asphalt. Part 1: Soluble Binder Content*; European Committee for Standardization: Brussels, Belgium, 2020.
36. European Committee for Standardization. *EN 933-9: Tests for Geometrical Properties of Aggregates. Part 9: Assessment of Fines—Methylene Blue Test*; European Committee for Standardization: Brussels, Belgium, 2010.
37. European Committee for Standardization. *EN 1097-3: Tests for Mechanical and Physical Properties of Aggregates. Part 3: Determination of Loose Bulk Density and Voids*; European Committee for Standardization: Brussels, Belgium, 1998.
38. European Committee for Standardization. *EN 196-6: Methods of Testing Cement—Part 6: Determination of Fineness*; European Committee for Standardization: Brussels, Belgium, 2018.
39. British Standards Institution. *EN 13808: Bitumen and Bituminous Binders—Framework for Specifying Cationic Bituminous Emulsions*; British Standards Institution: London, UK, 2013.
40. European Committee for Standardization. *EN 197-1: Cement—Composition, Specifications and Conformity Criteria for Common Cements*; European Committee for Standardization: Brussels, Belgium, 2011.
41. European Committee for Standardization. *EN 196-3: Methods of Testing Cement—Part 3: Determination of Setting Times and Soundness*; European Committee for Standardization: Brussels, Belgium, 2016.
42. European Committee for Standardization. *EN 196-1: Methods of Testing Cement—Determination of Strength*; European Committee for Standardization: Brussels, Belgium, 2016.
43. European Committee for Standardization. *EN 12850: Bitumen and Bituminous Binders—Determination of the pH Value of Bituminous Emulsions*; European Committee for Standardization: Brussels, Belgium, 2002.
44. European Committee for Standardization. *EN 1431: Bitumen and Bituminous Binders—Determination of Residual Binder and Oil Distillate from Bitumen Emulsions by Distillation*; European Committee for Standardization: Brussels, Belgium, 2009.
45. British Standards Institution. *EN 1429: Bitumen and Bituminous Binders—Determination of Residue on Sieving of Bituminous Emulsions, and Determination of Storage Stability by Sieving*; British Standards Institution: London, UK, 2013.
46. European Committee for Standardization. *EN 13075-1: Bitumen and Bituminous Binders—Determination of Breaking Behaviour—Part 1: Determination of Breaking Value of Cationic Bituminous Emulsions, Mineral Filler Method*; European Committee for Standardization: Brussels, Belgium, 2009.
47. European Committee for Standardization. *EN 12848: Bitumen and Bituminous Binders—Determination of Mixing Stability with Cement of Bituminous Emulsions*; European Committee for Standardization: Brussels, Belgium, 2009.
48. European Committee for Standardization. *EN 13074: Bitumen and Bituminous Binders—Recovery of Binder from Bituminous Emulsion or Cut-Back or Fluxed Bituminous Binders—Part 1: Recovery by Evaporation*; European Committee for Standardization: Brussels, Belgium, 2019.
49. European Committee for Standardization. *EN 1426: Bitumen and Bituminous Binders—Determination of Needle Penetration*; European Committee for Standardization: Brussels, Belgium, 2015.
50. European Committee for Standardization. *EN 1427: Bitumen and Bituminous Binders—Determination of the Softening Point—Ring and Ball Method*; European Committee for Standardization: Brussels, Belgium, 2011.
51. Azienda Autonoma di Stato per i Lavori Pubblici (AASLP). *Capitolato Speciale d'Appalto per la Manutenzione Straordinaria per Opere Stradali*; AASLP: San Marino, Italy, 2017. (In Italian)

52. European Committee for Standardization. *EN 12697-6: Bituminous Mixtures—Test Methods for Hot Mix Asphalt. Part 6: Determination of Bulk Density of Bituminous Specimens*; European Committee for Standardization: Brussels, Belgium, 2012.
53. European Committee for Standardization. *EN 12697-23: Bituminous Mixtures—Test Methods for Hot Mix Asphalt. Part 23: Determination of the Indirect Tensile Strength of Bituminous Specimens*; European Committee for Standardization: Brussels, Belgium, 2003.
54. Grilli, A.; Mignini, C.; Graziani, A. Field behaviour of cold-recycled asphalt mixtures for binder courses. In *Proceedings of the International Conference on Sustainable Materials, Systems and Structures (SMSS 2019)*, Rovinj, Croatia, 20–22 March 2019; pp. 100–107.
55. Deutsches Institut für Normung. *DIN 18134: Soil—Testing Procedures and Testing Equipment—Plate Load Test*; Deutsches Institut für Normung: Berlin, Germany, 2001.
56. European Committee for Standardization. *EN 12697-8: Bituminous Mixtures—Test Methods for Hot Mix Asphalt. Part 8: Determination of Void Characteristics of Bituminous Specimen*; European Committee for Standardization: Brussels, Belgium, 2018.
57. European Committee for Standardization. *EN 12697-26: Bituminous Mixtures—Test Methods for Hot Mix Asphalt. Part 26: Stiffness*; European Committee for Standardization: Brussels, Belgium, 2018.
58. Mignini, C.; Cardone, F.; Graziani, A. Experimental study of bitumen emulsion-cement mortars: Mechanical behaviour and relation to mixtures. *Mater. Struct.* **2018**, *51*, 149. [[CrossRef](#)]
59. Kim, Y.R. *Modeling of Asphalt Concrete*, 1st ed.; McGraw-Hill: New York, NY, USA, 2008.
60. Dolzycki, B.; Jaczewski, M.; Szydłowski, C. The long-term properties of mineral-cement-emulsion mixtures. *Constr. Build. Mater.* **2017**, *156*, 799–808. [[CrossRef](#)]
61. Gergesova, M.; Zupančič, B.; Saprunov, I.; Emri, I. The Closed Form t-T-P Shifting (CFS) Algorithm. *J. Rheol.* **2011**, *55*, 1–16. [[CrossRef](#)]
62. Sayegh, G. Viscoelastic Properties of Bituminous Mixtures. In *Proceedings of the 2nd International Conference on Structural Design of Asphalt Pavements*, Ann Arbor, MI, USA, 7–11 August 1967; pp. 743–755.
63. Genta, G. *Vibration Dynamics and Control*, 1st ed.; Springer: Boston, MA, USA, 2009.
64. Ashmawy, A.K.; Salgado, R.; Guha, S.; Drnevich, V.P. Soil damping and its use in dynamic analyses. In *Proceedings of the 3rd International Conference on Recent Advanced Geotechnical Earthquake Engineering and Soil Dynamics*, St. Louis, MI, USA, 2–7 April 1995.
65. Di Benedetto, H.; Olard, F.; Sauze'at, C.; Delaporte, B. Linear viscoelastic behaviour of bituminous materials: From binders to mixes. *Road Mater. Pavement Des.* **2004**, *5* (Suppl. 1), 163–202. [[CrossRef](#)]
66. Dongré, R.; Myers, L.; D'Angelo, J.; Paugh, C.; Gudimettla, J. Field evaluation of Witczak and Hirsch models for predicting dynamic modulus of hot-mix asphalt. *J. Assoc. Asph. Paving Technol.* **2005**, *74*, 381–442.
67. Pronk, A.C. The Huet–Sayegh model: A simple and excellent rheological model for master curves of asphaltic mixes. In *Proceedings of the Symposium on Mechanics of Flexible Pavements*, Baton Rouge, LA, USA, 1–3 June 2005.
68. Mangiafico, S.; Di Benedetto, H.; Sauze'at, C.; Olard, F.; Pouget, S.; Planque, L. Influence of reclaimed asphalt pavement content on complex modulus of asphalt binder blends and corresponding mixes: Experimental results and modelling. *Road Mater. Pavement Des.* **2013**, *14* (Suppl. 1), 132–148. [[CrossRef](#)]
69. Mangiafico, S.; Di Benedetto, H.; Sauze'at, C.; Olard, F.; Pouget, S.; Planque, L. New method to obtain viscoelastic properties of bitumen blends from pure and reclaimed asphalt pavement binder constituents. *Road Mater. Pavement Des.* **2014**, *15*, 312–329. [[CrossRef](#)]
70. Godenzoni, C.; Graziani, A.; Perraton, D. Complex modulus characterisation of cold-recycled mixtures with foamed bitumen and different contents of reclaimed asphalt. *Road Mater. Pavement Des.* **2017**, *18*, 130–150. [[CrossRef](#)]

Publisher's Note: MDPI stays neutral with regard to jurisdictional claims in published maps and institutional affiliations.



© 2020 by the authors. Licensee MDPI, Basel, Switzerland. This article is an open access article distributed under the terms and conditions of the Creative Commons Attribution (CC BY) license (<http://creativecommons.org/licenses/by/4.0/>).